(Received 27 April 2026, Accepted 7 July 2026, Scheduled 28 July 2026)

Performance and Complexity Analysis of Group-Connected Beyond-Diagonal RIS in Multi-User MIMO System

Huda A. Al-Tayyar*, Omar M. Ali, Reyam H. Ali, and Ali H. Saeed

Department of Communications and Intelligent Digital Systems Engineering, College of Engineering
University of Mosul, Mosul-41002, Iraq

ABSTRACT: Reconfigurable Intelligent Surfaces (RISs) have become a trend recently and represent a revolutionary development in wireless communication. Although RIS is utilized to enhance spectrum efficiency, particularly in Multi-User Multi-Input Multi-Output (MU-MIMO) environments, the conventional diagonal RIS (D-RIS) architecture represents a significant limitation. Beyond-diagonal RIS designs, such as fully-connected (FC-BD-RIS) and group-connected (GC-BD-RIS), are effective in controlling scattering and performance due to their use of reflective RIS elements. This research analyzes in detail the simulation of FC-BD-RIS, GC-BD-RIS, D-RIS, and baseline NO-RIS architectures assuming a real communication environment. The results show that the FC-BD-RIS architecture achieves the best performance and highest rate under all operational conditions, while the GC-BD-RIS architecture showed balanced and efficient performance relative to the computational complexity compared to the FC-BD-RIS. Ultimately, the behavior of per-user rate has demonstrated the ability of beyond-diagonal BD-RIS architectures to suppress interference and achieve fairness within MU-MIMO scenarios. Based on the results of this work, GC-BD-RIS is the most practical and suitable for future large-scale 6G applications. This work draws attention to the trade-off among design, optimization, and achievement of RIS-enabled MU-MIMO systems.

1. INTRODUCTION

The rapid development of Reconfigurable Intelligent Surface (RIS) technologies stems from their ability to reshape, redirect, or reflect electromagnetic waves towards specific areas with unprecedented flexibility [1]. All these characteristics are vital for multi-user MIMO systems, where increased dispersion, significant interference, and fluctuating propagation conditions limit their performance [2, 3].

Traditional D-RIS structures have limited ability to achieve spatial utilization freely due to the isolated phase shift of each element [4]. To address this issue, Beyond-Diagonal RIS (BD-RIS) structures have been proposed that provide better control through communication between their elements [5, 6]. The fully connected BD-RIS (FC-BD-RIS) architecture offers the most reconfiguration. On the other hand, the group-connected BD-RIS (GC-BD-RIS) architecture, based on the idea of dividing elements into smaller, interconnected groups, provides a distinct balance between system performance and complexity [7, 8]. In addition, RIS-aided systems must remain computationally scalable, resistant to Channel State Information (CSI) conditions, and capable of achieving fairness between users, especially in a crowded communications environment [9, 10]. Although many studies have focused on various system performance metrics, there is a lack of comprehensive research that addresses measurement, robustness, computational complexity, and sum rate within multi-user mobility [11, 12]. Therefore, this study aims to fill this knowledge gap and focuses on several valuable technical contributions that have not been sufficiently addressed in previous literature, including:

- Providing a unified comparative assessment within a unified MU-MIMO environment that covers D-RIS, FC-BD-RIS, and GC-BD-RIS architectures.
- An integrated investigation of the effect of RIS placement, scalability with RIS size, the impact of user mobility, computational complexity, fairness behavior, and robustness against CSI within a single study.
- Assuming a realistic MU-MIMO deployment that includes supported Rician RIS channels, path loss modelling, and precoding strategies.
- Incorporating a practical trade-off between performance and complexity in FC-BD-RIS and GC-BD-RIS architectures, which is highly relevant to scalable 6G RIS strategies.

The results show that the BD-RIS architectures, especially GC-BD-RIS, provide optimal performance while maintaining complexity management, making GC-BD-RIS a candidate for developers of smart 6G networks.

2. RELATED WORK

Recently, researchers have focused on the diagonal (D-RIS) technique with an individual phase shift for each reflective element [1, 2]. Although the D-RIS has control over structural constraints, some studies have achieved promising results in

* Corresponding author: Huda A. Al-Tayyar (huda.aqeel@uomosul.edu.iq).

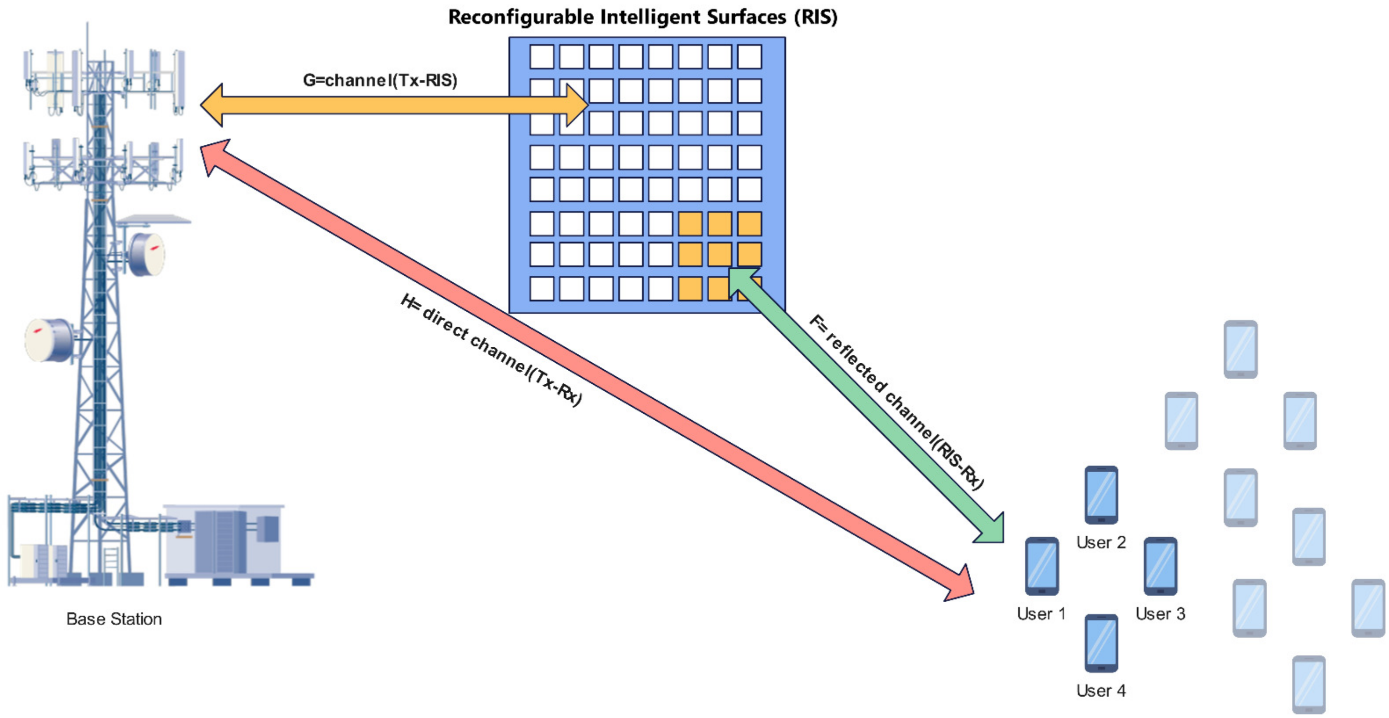

FIGURE 1. Direct BS-user link and RIS-enhanced transmission in a multi-user MIMO system.

terms of spectrum efficiency, improved coverage range, and reduced interference [4]. Beyond-diagonal RIS (BD-RIS) architectures have been proposed to overcome these challenges by utilizing switches, transmission lines, or tunable elements to improve inter-element coupling among the RIS elements [13]. The BD-RIS uses nondiagonal impedance or scattering arrays, which in turn enhances flexible beamforming and suppresses interference. However, the fully connected BD-RIS (FC-BD-RIS), where every element is connected, provides efficient handling of signals [14]. The practical and large-scale implementation of FC-BD-RIS has faced many critical challenges, such as increased device complexity and optimization factors [15, 16]. To overcome scalability limitations, group-connected BD-RIS (GC-BD-RIS) architectures have been proposed, where RIS elements are divided into small, interconnected groups [17]. However, current GC-BD-RIS studies focus on specific scenarios or performance metrics without providing a comprehensive comparison with traditional FC-BD-RIS and D-RIS under real-world, multi-user conditions.

Recent studies have demonstrated RIS-aided beamforming and multi-RIS deployment, primarily to improve remote-field positioning [18]. Furthermore, the scalability of large-scale passive RIS performance has been investigated [19], whereas the distinctive scalability characteristics of BD-RIS due to element coupling remain largely unexplored. Robust beamforming under (CSI) parameters in RIS-aided systems has been examined [20], but primarily for D-RIS or active beamforming configurations, with limited attention paid to the robustness evaluation of the BD-RIS. Finally, recent studies have highlighted the importance of algorithmic complexity and scalability in RIS-aided MU-MIMO systems [21]. Although previous studies have established frameworks for designing RIS and BD-RIS systems, a lack of comprehensive evaluation addressing performance, scalability, robustness under imperfect CSI, portability, equitable distribution, and computational complexity across various RIS architectures has been noted. This study aims to bridge this gap by providing a wide-ranging comparative analysis of FC-BD-RIS, GC-BD-RIS, D-RIS, and No-RIS baselines that examine multiple performance dimensions.

3. SYSTEM MODEL AND RIS ARCHITECTURES

It is considered a downlink multi-user multiple-input multiple-output (MU-MIMO) system in which a base station (BS) equipped with Nt antennas serves U multiple antenna users with the assistance of a reconfigurable intelligent surface (RIS) comprising M passive reflecting elements as shown in Fig. 1.

3.1. Network Geometry and Direct BS --- User Channel Model

Let positions of the BS, RIS, and user u be denoted by $\mathbf{p}_{BS}$, $\mathbf{p}_{RIS}$, and $\mathbf{p}_u \in \mathbb{R}^3$, respectively. The distance of the direct path is $d_{BU,u}$, and the cascaded paths are d_{BR} and $d_{RU,u}$. In the Large-scale fading model, the path loss follows the log-distance model used in most powerful RISs [22]:

$$\beta(d) = 10^{-\frac{\mathrm{PL}_0 + 10\alpha \log_{10}(d/d_0)}{10}}, \tag{1}$$

where PL_0 is the reference loss at distance d_0, and α is the path-loss exponent (distinct for direct and RIS-related links).

In small-scale fading, the BS-user u direct channels follow Rayleigh fading [23]:

$$\mathrm{h}_u = \sqrt{\beta_{BU,u}}\mathrm{h}_u^{ss} \quad \mathrm{h}_u^{ss} \sim \mathcal{CN}(0, \mathrm{I}_{N_t}) \tag{2}$$

The BS-RIS channel $\mathrm{G} \in \mathbb{C}^{M\times N_t}$ and RIS-user channel $\mathrm{F}_u \in \mathbb{C}^{M}$ follow Rician fading as validated in [1, 24]:

$$\mathrm{G} = \sqrt{\beta}_{BR}\left(\sqrt{\frac{K}{K+1}}\mathrm{G}^{LOS}+\sqrt{\frac{1}{K+1}}\mathrm{G}^{NLOS}\right), \quad (3)$$

$$\mathrm{F}_u = \sqrt{\beta}_{RU,u}\left(\sqrt{\frac{K}{K+1}}\mathrm{F}_u^{LOS}+\sqrt{\frac{1}{K+1}}\mathrm{F}_u^{NLOS}\right), \quad (4)$$

where K is the Rician factor.

3.2. RIS Architectures

Let $\Theta \in C^{\mathrm{M}\times\mathrm{M}}$ denote the RIS transformation matrix and M denote the number of RIS elements. Three architectures are considered with RIS mathematical updating derivation, computational complexity, and convergence analysis.

1) Conventional Diagonal RIS (D-RIS)

The conventional RIS applies independent phase shifts per element.

$$\Theta_D = \mathrm{diag}(e^{j\theta_1}, \ldots, e^{j\theta_M}). \quad (5)$$

where $\theta_{\mathrm{m}} \in [0, 2\pi)$ denotes the phase shift of reflecting elements. Assuming the transmitting precoder $W = [w_1, \ldots, w_{\mathrm{u}}]$, the received signal at RIS element S_{m} can be represented by:

$$S_m = \sum_{u=1}^{U} f_{u,m} g_m w_u \quad (6)$$

where $f_{u,m}$ is the RIS-user channel coefficient, g_m the vector of BS-RIS channel, and w_u the beamforming vector for each RIS element. Optimizing the RIS system involves maximizing the reflected signal by upgrading the element phase with the contribution of the effective cascaded channel, resulting in:

$$\theta_m^* = -\angle S_m, \quad m = 1, \ldots, M. \quad (7)$$

By substituting (7) into (5), the reflected signals are constructively combined at the receivers, increasing the gain of the current precoder. The RIS and BS precoder parameters are then alternately updated until the target convergence of sum rate is achieved. This structure offers low complexity, described as $\mathcal{O}(M)$ but limited spatial controllability [22].

2) Fully-connected beyond-diagonal RIS (FC-BD-RIS)

The FC-BD-RIS allows interaction between elements via a tunable impedance network, enabling a fully-connected transformation matrix. The fully-connected BD-RIS matrix (which is not limited to a diagonal structure) can be modeled as:

$$\Theta_{\mathrm{FC}} = [\theta_{m,n}]_{M\times M}, \quad \theta_{m,n} = \text{complex coupling between elements} \quad (8)$$

This architecture maximizes flexible control over both self-reflection and inter-element coupling compared with the D-RIS architecture, but incurs high complexity $\mathcal{O}(M^3)$ [16]. The FC-BD-RIS system can be improved by maximizing all reflected paths, i.e., $\max_{\Theta_{\mathrm{FC}}}\{\mathrm{sum}(\Theta_{\mathrm{FC}}^H S)\}$. The optimum phase projection is achieved by aligning each element of Θ_{FC} with the corresponding element of S, resulting in

$$\Theta_{\mathrm{FC}}^* = e^{-j\angle(S)} \quad (9)$$

Equation (9) provides an update to the FC-BD-RIS, the BS precoder alternately, and the contribution of reflected signals to the current beamforming until sum rate convergence is achieved.

3) Group-connected BD-RIS (GC-BD-RIS)

A practical implementation reduces complexity by grouping RIS elements into G groups of size $M_g = M/G$:

$$\Theta_{GC} = \mathrm{blkdiag}(\Theta_1, \ldots, \Theta_G), \quad \Theta_g \in \mathbb{C}^{M_g\times M_g}. \quad (10)$$

Each block satisfies electromagnetic element coupling, but no coupling occurs between groups. The resulting complexity makes GC-BD-RIS far more scalable as [13]:

$$\mathcal{C}_{GC} = G\cdot\mathcal{O}(M_g^2) = \mathcal{O}\left(\frac{M^2}{G}\right), \quad (11)$$

The optimization here remains identical to that in FC-BD-RIS, at a fixed transmitting precoder, except for the effectiveness of the Θ_{GC} in the GC-BD structure. Accordingly, the effective channel corresponding to the g group is defined as:

$$Sg = \sum_{u=1}^{U} (G_g w_u) f_{u,g} \quad (12)$$

Every channel component in (12) is associated with the g group. As a result, the optimization at each block group will be max_$\Theta_{\mathrm{GC}}\{sum(\Theta_{\mathrm{g}}^H S_g)\}$. The phase alignment in GC-BD-RIS follows the same basis as FC-BD-RIS in a block form:

$$\Theta_g^* = e^{-j\angle(S_g)}, \quad g = 1, \ldots, G \quad (13)$$

The GC-BD-RIS matrix is optimized by combining all optimized blocks according to (10). It provides a compromise between D-RIS and FC-BD-RIS technologies in terms of limited flexibility and high complexity, while retaining a significant portion of the performance improvements.

3.3. Composite BS-RIS-User Effective Channel

For user u, the reflected BS→RIS→user channel is [25]:

$$\mathrm{h}_u^{(RIS)} = \mathrm{F}_u^T \Theta G. \quad (14)$$

yielding the effective channel:

$$\mathrm{h}_u^{(eff)} = \mathrm{h}_{B,u} + \mathrm{h}_u^{(RIS)} \quad (15)$$

Collecting all users:

$$\mathrm{H}_{\mathit{eff}} = \begin{bmatrix} (\mathrm{h}_1^{eff})^T \\ \vdots \\ (\mathrm{h}_U^{eff})^T \end{bmatrix} \in \mathbb{C}^{U\times N_t} \quad (16)$$

This integrated construction is suitable for all RIS architectures.

3.4. Imperfect Channel State Information CSI Model

Channel state information (CSI) is usually unavailable in most operational systems because of quantization, estimation, and feedback suspensions. Following the standard RIS-assisted MU-MIMO models, the estimated effective channel is modeled as:

$$\hat{H}_{\mathit{eff}} = H_{\mathit{eff}} + E \quad (17)$$

where $E \in C^{U \times Nt}$ denotes the CSI error matrix with independent and identically distributed entries following $\mathcal{CN}(0, \epsilon)$. Parameter ϵ represents the normalized mean square error (NMSE). The BS designs its precoder based on $\hat{\mathbf{H}}_{\mathbf{eff}}$, while the performance metrics are evaluated using the true channel, H_{eff} [26]. The adopted CSI-based Gaussian distribution model has provided a practical representation of channel uncertainty. Furthermore, it can be interpreted as a probabilistic model equivalent to finite elliptic uncertainty sets through confidence area analysis. Given the system geometry and antenna spacing, spatial error correlations are expected to be limited; therefore, the proposed framework remains representative of a more general CSI model. Besides that, the observed performance superiority of non-diagonal RIS structures is expected to remain unchanged.

4. PROBLEM FORMULATION AND OPTIMIZATION FRAMEWORK

Given the non-convex coupling between the transmission precoder and the RIS, the optimization of the precoding matrix and RIS is iteratively performed using the Alternate Optimization (AO) approach as detailed in this section. Let $\mathbf{W} = [\mathbf{w}_1, \ldots, \mathbf{w}_U] \in \mathbb{C}^{N_t \times U}$ denote the linear precoding matrix at the BS, where w_u is the beamforming vector intended for user u [27]. The received signal at user u is:

$$y_u = \mathrm{h}_u^{eff} w_u s_u + \sum_{i \neq u} \mathrm{h}_u^{eff} w_i s_i + n_u \tag{18}$$

where h_u^{eff} is defined in Section 3, s_u is the transmitted symbol with $\mathbb{E}[|s_u|^2] = 1$, and $n_u \sim \mathcal{CN}(0, \sigma^2)$ is the additive white Gaussian noise. The corresponding Signal to Interference and Noise Ratio (SINR) and rate are

$$\gamma_u(W, \Theta) = \frac{|\mathrm{h}_u^{eff}(\Theta) w_u|^2}{\sum\limits_{i \neq u} |\mathrm{h}_u^{eff}(\Theta) w_i|^2 + \sigma^2} \tag{19}$$

$$R_u(W, \Theta) = \log_2(1 + \gamma_u) \tag{20}$$

and the system sum rate is

$$R_{\text{sum}}(W, \Theta) = \sum_{u=1}^{U} R_u(W, \Theta) \tag{21}$$

The joint design problem is formulated as

$$\max_{W, \Theta} R_{\text{sum}}(W, \Theta) = \sum_{u=1}^{U} R_u(W, \Theta) \tag{22}$$

This joint optimization is highly non-convex owing to the coupled effects of W and Θ and the unit modulus constraints [16, 27].

Given a fixed RIS configuration Θ, the effective channel matrix H_{eff} is determined. To mitigate multi-user interference with manageable complexity, zero-forcing (ZF) precoding has been adopted, which is widely used in MU-MIMO systems and RIS-assisted networks. The ZF precoder is expressed as

$$W = H_{\mathit{eff}}^H \left(H_{\mathit{eff}} H_{\mathit{eff}}^H\right)^{-1} \tag{23}$$

followed by power normalization to satisfy the transmit power constraint:

$$W = \sqrt{\frac{P_T}{\text{tr}(WW^H)}} W \tag{24}$$

ZF precoding eliminates inter-user interference under perfect CSI and provides a favorable balance between performance and computational complexity, making it suitable for large-scale RIS-assisted systems.

The overall Alternating Optimization (AO) procedure can be summarized as follows:

1. **Initialization**:
   - Initialize $\Theta^{(0)}$ (random phases or heuristic BD-RIS structure).
   - Compute $W^{(0)}$ via ZF for $\Theta^{(0)}$.
2. **Repeat for** $t = 0, 1, \ldots, T_{\text{max}}$:
   - **Step 1 (Precoder update)**:

     $W^{(t|1)} \leftarrow W\left(\Theta^{(t)}\right)$ using ZF + power normalization.
   - **Step 2 (RIS update)**:

     Update $\Theta^{(t+1)}$ using: Element-wise phase alignment (D-RIS), Matrix-level phase projection (FC-BD-RIS), or Block-wise projection (GC-BD-RIS).
   - Evaluate $R_{\text{sum}}^{(t|1)}$.
3. **Stopping Criterion**:

Terminate when the relative increase in sum-rate $|R_{\text{sum}}^{(t|1)} - R_{\text{sum}}^{(t)}|/R_{\text{sum}}^{(t)}$ falls below a given threshold or when the maximum number of iterations is reached. AO is known to converge to high-quality stationary points in RIS-assisted systems. In all simulated scenarios, the proposed framework exhibited a stable convergence behavior with moderate iteration counts. In our simulations, the algorithm converged within a moderate number of iterations and exhibited stable behavior under all considered scenarios (signal-to-noise ratio (SNR) sweeps, RIS size scaling, mobility, and CSI errors) as shown in Section 5.

5. NUMERICAL RESULTS AND DISCUSSION

This section presents a thorough numerical evaluation of the proposed RIS-aided MU-MIMO system over a wide range of operating conditions. All simulations considered a downlink scenario with $U = 4$ users, $N_t = 4$ transmitting antennas, and

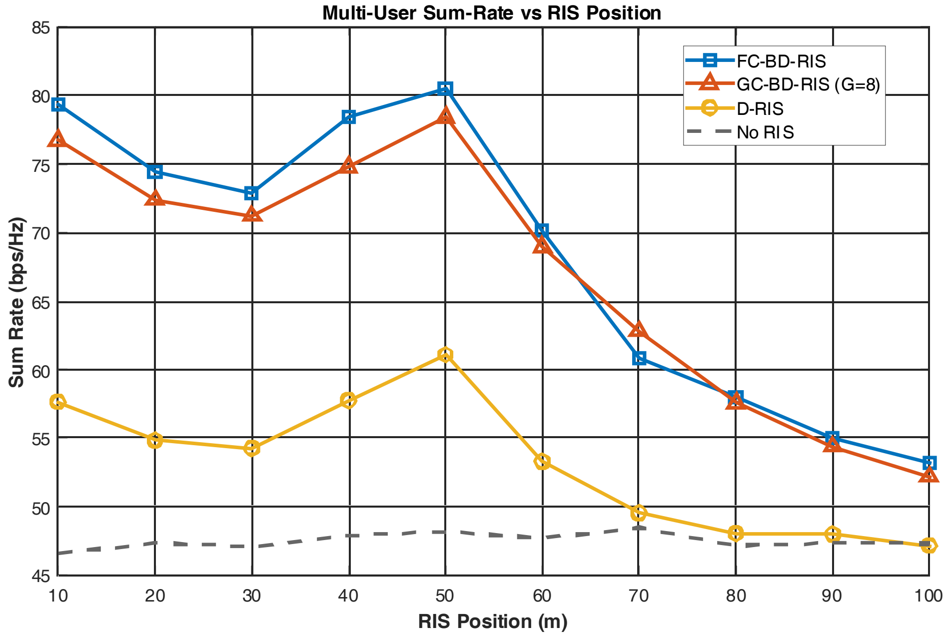

FIGURE 2. Sum-Rate vs. RIS Position at 4 architectures (FC_BD_RIS, GC_BD_RIS, D_RIS, and No RIS).

$N_r = 4$ receiving antennas per user. The RIS elements follow a Rician fading model and realistic large-scale path-loss parameters calibrated from recent experimental studies. For each configuration, Monte Carlo averaging is performed across 100 fading realizations.

5.1. Sum Rate vs. RIS Position:

Figure 2 investigates the impact of the RIS location on the system sum rate under fixed system parameters for different RIS architectures.

- The **FC-BD-RIS** provides the highest sum rate across RIS positions, owing to the full connectivity of the network, which emphasizes the flexibility of beamforming in addition to multi-user interference-efficient management.
- **GC-BD-RIS** follows the performance of FC-BD-RIS while reducing the computational complexity. This is an attractive practical alternative.
- The **diagonal RIS (D-RIS)** performs better than the no-RISscenario; however, limited phase-only control prevents it from efficiently utilizing the RIS positions.
- **No-RIS** shows the lowest sum rate, which indicates the vital role of an RIS-aided system.

FC-BD-RIS has achieved the highest sum rate of 80.5 bps/Hz, followed by GC-BD-RIS (78 bps/Hz), and D-RIS (61 bps/Hz), with the lowest rate at No-RIS (48 bps/Hz) when the RIS is positioned at 50 m. Furthermore, the results show that adopting an RIS approach has a significant impact on system performance.

5.2. Sum Rate vs. SNR

The performance under a specified transmission power and a fixed RIS position was determined as a function of system SNR as illustrated in Fig. 3.

- **FC-BD-RIS** attains the highest sum rate owing to its fully scattering structure, allowing for the greatest spatial control.
- **GC-BD-RIS** provides a practical compromise between hardware complexity and good performance.
- **Diagonal RIS** has limited phase-control levels of independence but offers moderate gains.
- **No-RIS** confirms the need for RIS support by producing the lowest rate curves.

At a 15 dB-SNR, FC-BD-RIS increased the sum rate by 25% compared to GC-BD-RIS and by 134% compared to D-RIS.

Increasing the number of Monte Carlo realizations (100, 300, 500) results in slight differences in the sum rate, as shown in Table 1, which confirms the statistical stability of the proposed model.

TABLE 1. Sum rate versus the number of Monte Carlo realizations at SNR = 15 dB.

Monte Carlo realization	FC-BD RIS	GC-BD-RIS	D-RIS
100	36.89	30.42	15.5
300	36.1	30.4	15.89
500	36.03	30.04	15.51

5.3. Sum Rate vs. Number of RIS Elements M

Figure 4 shows the analysis of system performance with an increase in the sum rate and increasing M for all RIS structures.

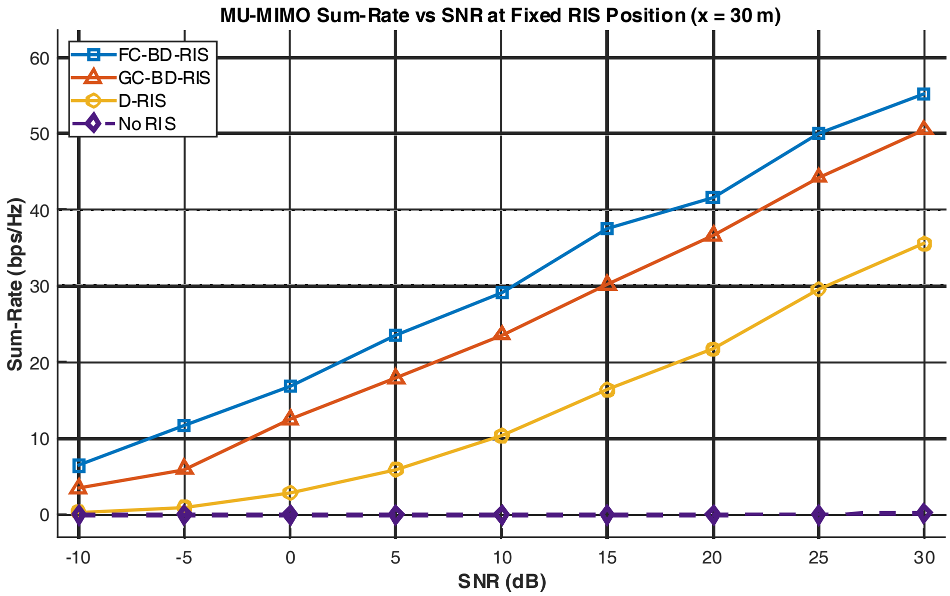

FIGURE 3. Sum rate vs. SNR at 4 architectures (FC_BD_RIS, GC_BD_RIS, D_RIS, and No RIS).

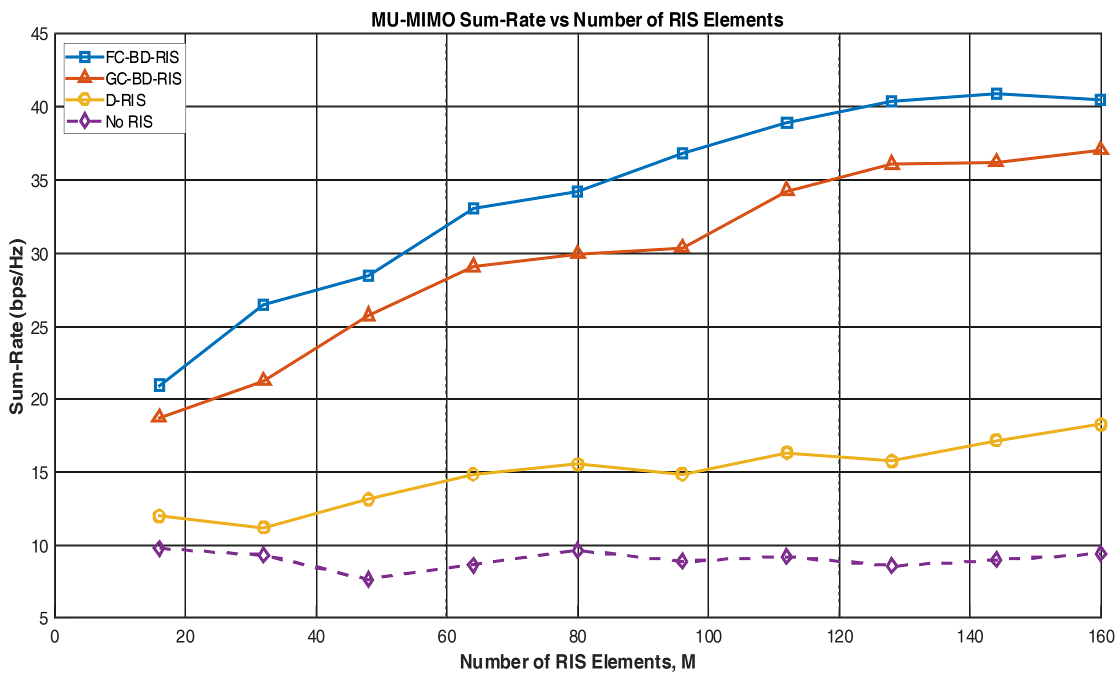

FIGURE 4. Sum rate vs. RIS size (M) for 4 architectures: (FC_BD_RIS, GC_BD_RIS, D_RIS, and No RIS).

- **FC-BD-RIS** utilizes its quadratic number of controllable coefficients to achieve the greatest effectiveness.
- **GC-BD-RIS** outperforms the RIS system even at a medium M value, while maintaining a stable balance between performance and complexity.
- **Diagonal RIS** shows a decrease in performance at a large RIS size. This behavior arises because a larger RIS provides higher passive beamforming gain, while the reflected MU-interference also increases. Consequently, the additional beamforming gain is partially offset by the residual interference, leading to performance saturation and, in some cases, a slight degradation. In contrast, FC-BD-RIS and GC-BD-RIS can exploit beyond-diagonal coupling to better suppress interference and utilize the increased RIS aperture more efficiently.
- **No-RIS** confirms the need for RIS integration by producing the lowest-growing sum-rate curve.

The architectural benefits of the BD-RIS models are evident when, for example, FC-BD-RIS achieved sum rate of 40.5 bps/Hz at 128 elements, surpassing GC-BD-RIS

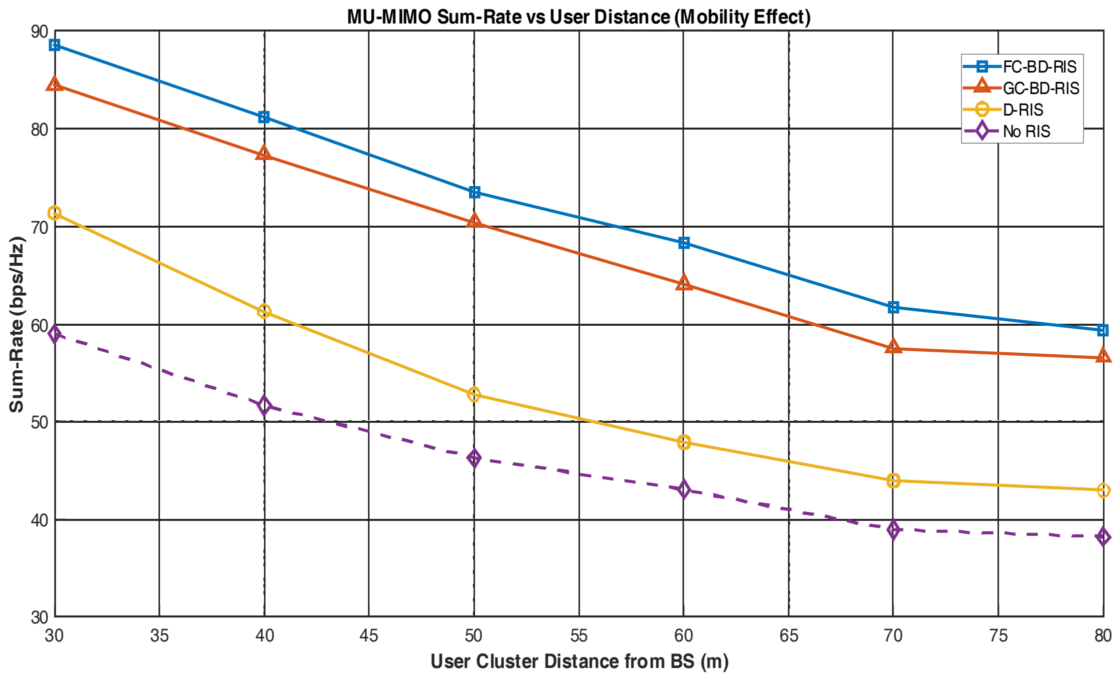

FIGURE 5. Sum rate vs. users' movement from BS for 4 architectures: (FC_BD_RIS, GC_BD_RIS, D_RIS, and No RIS).

(36 bps/Hz), D-RIS (15.9 bps/Hz), and No-RIS (8.7 bps/Hz) from the trends in the results.

5.4. Mobility Analysis: Sum Rate vs User Distance

Figure 5 illustrates the movement modeling along the Line-of-Sight (LOS) axis and assesses user movement and its effect on system robustness. The results show a decrease with distance owing to the increasing path loss.

- **FC-BD-RIS** exhibits greater resistance to geometric defects and maintains high rates for all distances.
- **GC-BD-RIS** follows FC-BD-RIS with slightly lower performance.
- **Diagonal RIS** provides minimal compensation for the path loss caused by user movement.
- **No-RIS** shows the lowest rate, which again demonstrates the need to use a system supported by the RIS.

These results show the necessary geometric robustness for real-world user mobility scenarios. For example, at 50 m BS-user distance, FC-BD-RIS outperforms GC-BD-RIS, D-RIS and NO-RIS models by approximately 4.3%, 37.4%, and 59.8%, respectively.

5.5. Per-User Rate Distribution

A bar plot of each user's rate is shown in Fig. 6, illustrating the fairness and quality of service per user.

- **FC-BD-RIS** demonstrates higher rates due to the ability to reduce interference for each user.
- **GC-BD-RIS** outperforms the diagonal-RIS index despite decreasing matrix connectivity.
- **Diagonal RIS** provides inconsistent rates, giving preference to users located closest to the RIS.
- **No-RIS** indicates the need for an RIS in balancing a MU-MIMO system.

To further quantify fairness measurement, Jain's fairness index (JFI) was used and defined as $J = \frac{(\sum_{i=1}^{U} R_i)^2}{U \sum_{i=1}^{U} R_i^2}$. The calculated JFI was approximately 1 for all RISs, confirming that the adopted ZF precoding provides near-perfect fairness across all RIS architectures considered.

5.6. Sum Rate under CSI Errors (Robustness Evaluation under Imperfect CSI)

The analysis of robustness performance against estimation errors is shown in Fig. 7. A controlled CSI error factor ϵ was injected into all channels. The results show that all RIS architectures experience a decrease in the rate as ϵ increases.

- **FC-BD-RIS** remains the most powerful performance, owing to its rich integrated structure that minimizes defects.
- **GC-BD-RIS** also shows strong robustness and outperforms the diagonal RIS throughout the CSI error range.
- **A Diagonal RIS** is highly sensitive to the CSI mismatch and degrades rapidly because of its limited degree of freedom.
- **No-RIS**, its performance was noticeably worse, as it was the least responsive.

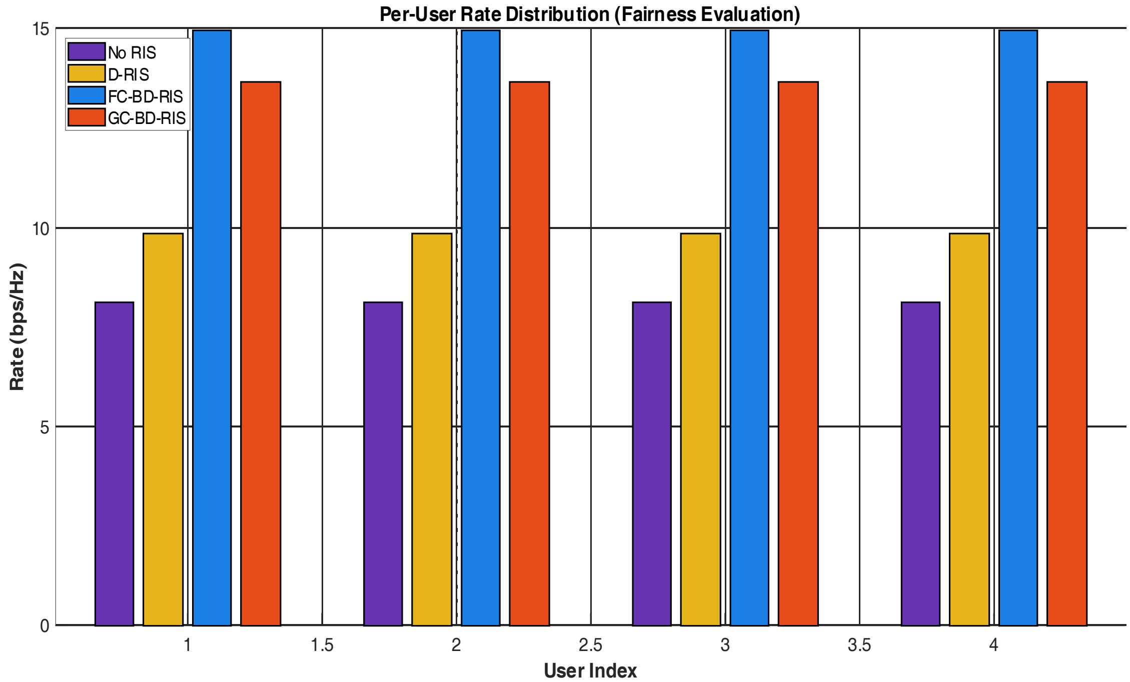

FIGURE 6. Per-user rate distribution (fairness evaluation).

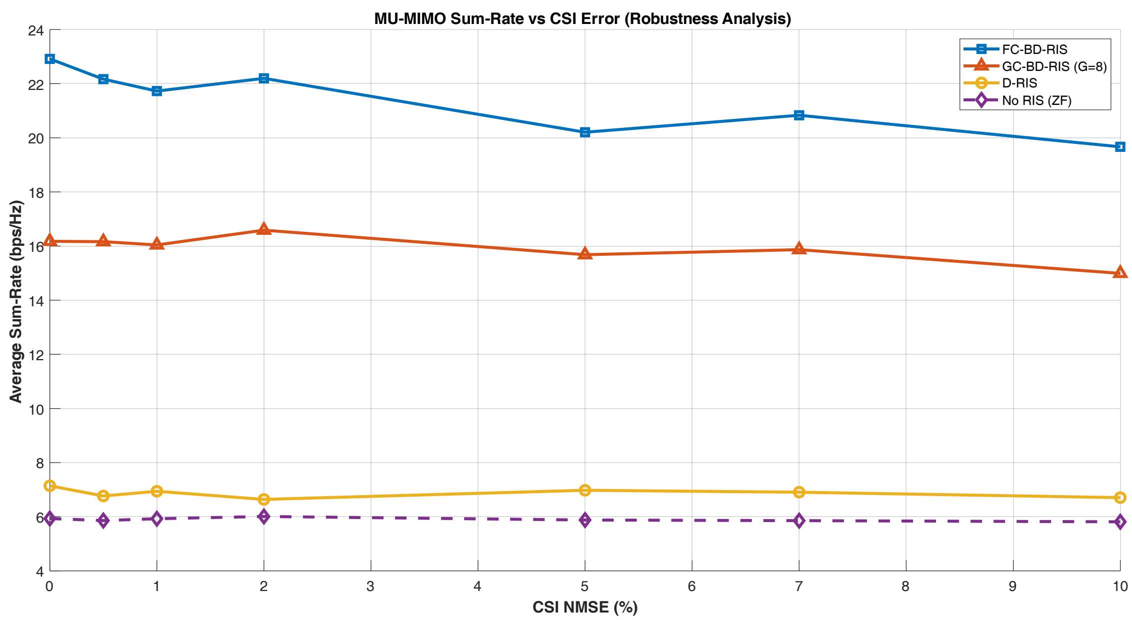

FIGURE 7. Sum rate vs. CSI error (robustness under imperfect CSI).

At 5% CSI error, FC-BD-RIS has been achieved a 25.8% and 185.7% higher sum rate than GC-BD-RIS and D-RIS, respectively. These patterns indicate the potential use of BD-RIS due to its inherent robustness.

5.7. Computational Complexity Comparison

Figure 8 illustrates the standard computational complexity of different RIS structures. The observed hierarchy:

$$\mathrm{D-RIS} \ll \mathrm{GC-BD-RIS} \ll \mathrm{FC-BD-RIS}$$

matches theoretical complexity orders:

- D-RIS: $\mathcal{O}(M)$
- GC-BD-RIS: $\mathcal{O}(M^2/G)$
- FC-BD-RIS: $\mathcal{O}(M^2)$

The Big-O expression was adopted to compare the computational complexity, while implementation-dependent runtime was not taken into account, as it varies according to the software

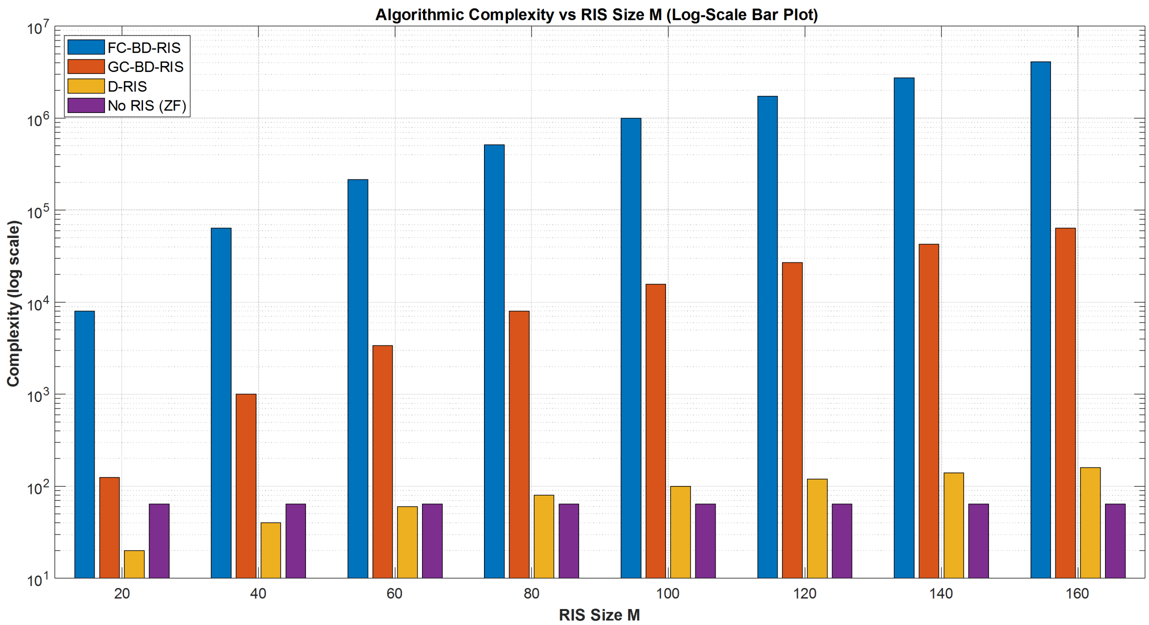

FIGURE 8. Algorithmic complexity comparison vs. RIS size M at 4 architectures (FC_BD_RIS, GC_BD_RIS, D_RIS, and No RIS).

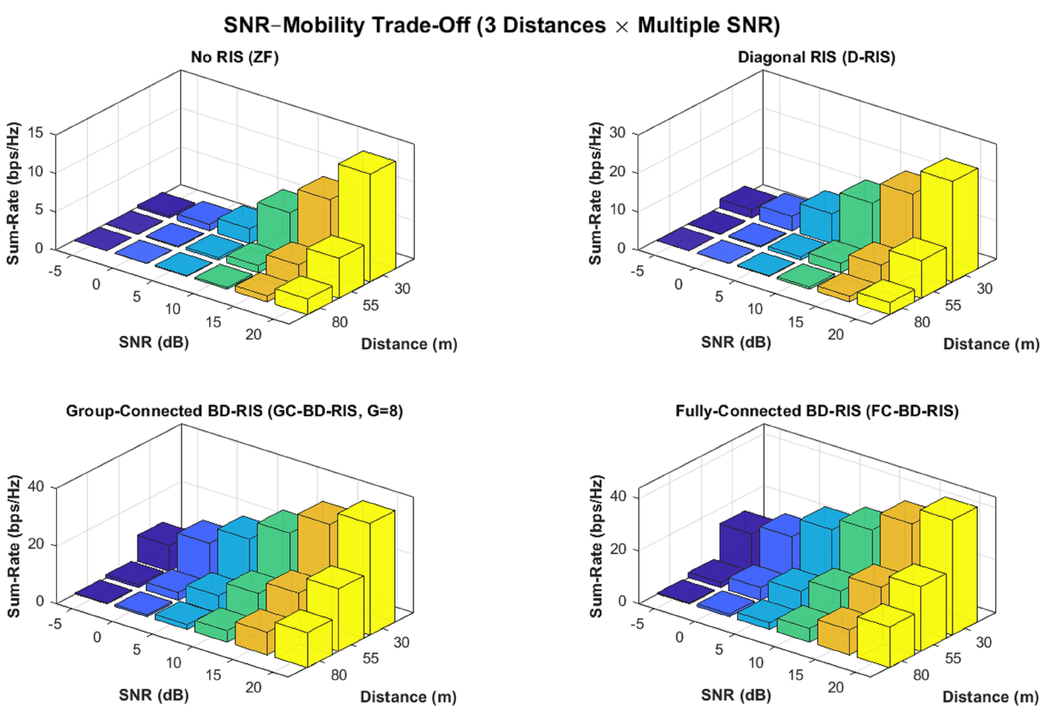

FIGURE 9. SNR-mobility trade-off for different RIS architectures.

environment and computing platform. It should be noted that the superior performance of FC-BD-RIS in sum rate has come at the cost of increased device connections, insertion losses, switching network, and computational complexity, which has led to higher power consumption. This demonstrates that the GC-BD-RIS offers a desirable compromise between computation efficiency and performance regardless of runtime and computing platform.

5.8. Robustness to SNR-Mobility Trade-Off

Apart from the fairness analysis in Fig. 6, this section examines the achievable sum rate under different user distances (30–80 m) and SNR (−5–20 dB), as in Fig. 9. An SNR scan was performed by varying the transmission power relative to a large-scale reference channel gain while maintaining a constant thermal noise power to ensure consistency with previous assessments. The results demonstrate that the differences between the

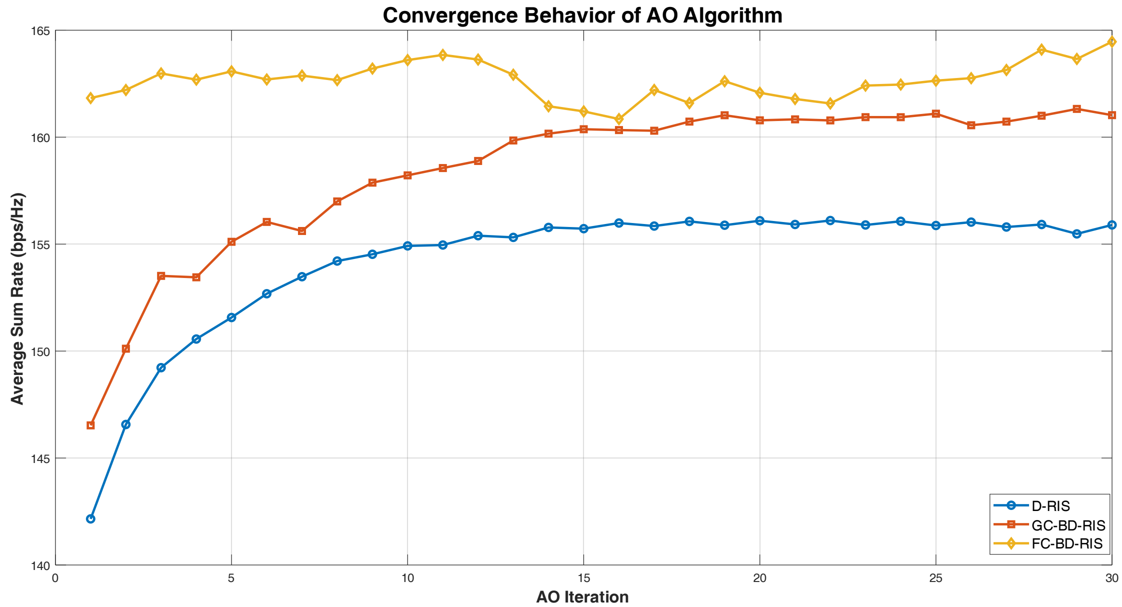

FIGURE 10. Convergence behavior of the AO algorithm for different RIS architectures.

TABLE 2. Comparative overview of RIS architectures and research scope.

Ref.	RIS Architecture	System Model	RIS Coupling Model	Placement Analysis	Scaling w.r.t. RIS Size	Robustness/CSI
[1, 2]	D-RIS	SISO/MISO	Diagonal (independent phase shifts)	✗	✓ (passive scaling)	✗
[4]	D-RIS	MISO	Diagonal	✗	✗	✗
[13]	BD-RIS (general)	SISO	Generic impedance matrix	✗	✗	✗
[14]	FC-BD-RIS	SISO	Fully connected	✗	✗	✗
[15, 16]	FC-BD-RIS	MISO	Fully connected	✗	✓	✗
[17]	GC-BD-RIS	Single-user	Group-connected	✗	✗	✗
[19]	D-RIS	MISO	Diagonal	✗	✓	✗
[20]	D-RIS	MU-MIMO	Diagonal	✗	✗	✓
[21]	D-RIS/Active	MU-MIMO	Diagonal/Active	✗	✗	✗
[28, 29]	D-RIS	SISO/MISO	Diagonal	✓	✗	✗
This work	D-RIS/GC-BD-RIS/FC-BD-RIS	MU-MIMO	Diagonal, Group, Fully-Connected	✓	✓	✓

RIS architectures become apparent with increasing SNR. Diagonal RIS systems are also highly affected by mobility, which can sometimes lead to reduced performance gains at long distances. Despite fluctuations in SNR and distance, the BD-RIS demonstrated stable performance.

5.9. Convergence of the Proposed AO Framework

The total sum rate has been recorded as a function of the number of Alternative Optimization (AO) iterations to demonstrate the convergence achieved in RIS architectures. Each AO iteration alternately optimizes the RIS matrix and ZF precoder, with each update corresponding to the adopted target function until convergence is reached. Fig. 10 shows the progressive convergence and stable behavior over a limited number of AO iterations under the proposed MU-MIMO environment conditions with a maximum of 30 AO iterations and a 10^{-4} convergence threshold. The FC-BD-RIS achieves the highest sum rate, followed by the GC-BD-RIS, and then the D-RIS design, thanks to its high flexible beamforming. This indicates that the adopted AO algorithm efficiently achieves an optimal solution.

These results show that GC-BD-RIS represents a significant improvement over classic RIS architectures and delivers a nearoptimal balance, achieving a performance close to that of FC-BD-RIS with drastically reduced complexity, especially for upcoming 6G MU-MIMO deployments that need to be robust, scalable, fair, and high capacity. Table 2 compares recent studies with the current research scope.

6. CONCLUSION

This paper has analyzed MU-MIMO systems supported by reconfigurable intelligent surfaces (RISs) working with beyond-diagonal (BD) architectures. A unified comparative framework was developed to evaluate diagonal RIS, group-connected BD-RIS (GC-BD-RIS), and fully-connected BD-RIS (FC-BD-RIS) systems in a common alternating optimization framework combining ZF-based precoding. The results presented sum-rate enhancements with increasing SNR and RIS size. In addition, both GC-BD-RIS and FC-BD-RIS have shown improved robustness in user mobility, distribution, and CSI inadequacy, providing robust performance under diverse conditions. Overall, the results show that GC-BD-RIS is the most practical and desirable configuration, allowing for efficient wave manipulation, better interference suppression, and improved fairness in MU-MIMO systems. Although this study is based on ZF precoding under ideal RIS hardware assumptions, future work may investigate advanced robust beamforming schemes, such as MMSE and WMMSE, together with practical hardware impairments to further improve BD-RIS performance in MU-MIMO systems. Future work may expand the proposed architecture to include collaborative multi-RIS deployments and active-passive hybrid RIS. The promising results of this study demonstrate the great potential of GC-BD-RIS architecture as a critical enabler for future intelligent wireless communication systems.

REFERENCES

[1] Huang, C., A. Zappone, G. C. Alexandropoulos, M. Debbah, and C. Yuen, "Reconfigurable intelligent surfaces for energy efficiency in wireless communication," *IEEE Transactions on Wireless Communications*, Vol. 18, No. 8, 4157–4170, 2019.

[2] Tang, W., M. Z. Chen, X. Chen, J. Y. Dai, Y. Han, M. D. Renzo, Y. Zeng, S. Jin, Q. Cheng, and T. J. Cui, "Wireless communications with reconfigurable intelligent surface: Path loss modeling and experimental measurement," *IEEE Transactions on Wireless Communications*, Vol. 20, No. 1, 421–439, 2021.

[3] Al Janaby, A., H. Al-Rizzo, and Y. Qassim, "Enhancing spectral efficiency of 6G downlink beamforming via cooperative multi-agent deep reinforcement learning," *Sensors*, Vol. 26, No. 3, 950, Feb. 2026.

[4] Di Renzo, M., A. Zappone, M. Debbah, M.-S. Alouini, C. Yuen, J. D. Rosny, and S. Tretyakov, "Smart radio environments empowered by reconfigurable intelligent surfaces: How it works, state of research, and the road ahead," *IEEE Journal on Selected Areas in Communications*, Vol. 38, No. 11, 2450–2525, 2020.

[5] Li, H., M. Nerini, S. Shen, and B. Clerckx, "Beyond diagonal reconfigurable intelligent surfaces in wideband OFDM communications: Circuit-based modeling and optimization," *IEEE Transactions on Wireless Communications*, Vol. 24, No. 4, 3623–3636, 2025.

[6] Li, H., S. Shen, and B. Clerckx, "Beyond diagonal reconfigurable intelligent surfaces: From transmitting and reflecting modes to single-, group-, and fully-connected architectures," *IEEE Transactions on Wireless Communications*, Vol. 22, No. 4, 2311–2324, 2023.

[7] Fang, T. and Y. Mao, "A low-complexity beamforming design for beyond-diagonal RIS aided multi-user networks," *IEEE Communications Letters*, Vol. 28, No. 1, 203–207, 2024.

[8] Nerini, M., S. Shen, and B. Clerckx, "Static grouping strategy design for beyond diagonal reconfigurable intelligent surfaces," *IEEE Communications Letters*, Vol. 28, No. 7, 1708–1712, 2024.

[9] Gao, M., J. Yang, H. Li, and Y. Wang, "Robust beamforming optimization design for RIS-aided MIMO systems with practical phase shift model and imperfect CSI," *IEEE Internet of Things Journal*, Vol. 11, No. 1, 958–973, 2024.

[10] Yang, Y., S. Dang, M. Wen, B. Ai, and R. Q. Hu, "Blockage-aware robust beamforming in RIS-aided mobile millimeter wave MIMO systems," *IEEE Transactions on Wireless Communications*, Vol. 23, No. 11, 16 906–16 921, 2024.

[11] Zhang, Y., J. Zhang, D. W. K. Ng, H. Xiao, and B. Ai, "Performance analysis of reconfigurable intelligent surface assisted systems under channel aging," *Intelligent and Converged Networks*, Vol. 3, No. 1, 74–85, 2022.

[12] Liu, Y., X. Liu, X. Mu, T. Hou, J. Xu, M. D. Renzo, and N. Al-Dhahir, "Reconfigurable intelligent surfaces: Principles and opportunities," *IEEE Communications Surveys & Tutorials*, Vol. 23, No. 3, 1546–1577, 2021.

[13] Nerini, M., S. Shen, H. Li, and B. Clerckx, "Beyond diagonal reconfigurable intelligent surfaces utilizing graph theory: Modeling, architecture design, and optimization," *IEEE Transactions on Wireless Communications*, Vol. 23, No. 8, 9972–9985, 2024.

[14] Li, H., S. Shen, M. Nerini, M. D. Renzo, and B. Clerckx, "Beyond diagonal reconfigurable intelligent surfaces with mutual coupling: Modeling and optimization," *IEEE Communications Letters*, Vol. 28, No. 4, 937–941, 2024.

[15] Nerini, M., S. Shen, H. Li, M. D. Renzo, and B. Clerckx, "A universal framework for multiport network analysis of reconfigurable intelligent surfaces," *IEEE Transactions on Wireless Communications*, Vol. 23, No. 10, 14 575–14 590, 2024.

[16] Santamaria, I., M. Soleymani, E. Jorswieck, and J. Gutiérrez, "MIMO capacity maximization with beyond-diagonal RIS," in *2024 IEEE 25th International Workshop on Signal Processing Advances in Wireless Communications (SPAWC)*, 936–940, Lucca, Italy, 2024.

[17] Samy, M., H. Al-Hraishawi, M. Alsenwi, A. B. M. Adam, S. Chatzinotas, and B. Ottersten, "Group-connected non-diagonal RIS: An energy efficiency analysis," *IEEE Wireless Communications Letters*, Vol. 14, No. 9, 2987–2991, 2025.

[18] Alhafid, A. K., S. Younis, and Y. E. M. Ali, "Enhanced far-field localization scheme using multi-RIS and efficient beam sweeping," *Progress In Electromagnetics Research C*, Vol. 140, 163–175, 2024.

[19] Zhang, P., J. Zhang, H. Xiao, H. Du, D. Niyato, and B. Ai, "RIS-aided 6G communication system with accurate traceable user mobility," *IEEE Transactions on Vehicular Technology*, Vol. 72, No. 2, 2718–2722, 2023.

[20] Basharat, S., M. Khan, M. Iqbal, U. S. Hashmi, S. A. R. Zaidi, and I. Robertson, "Exploring reconfigurable intelligent surfaces for 6G: State-of-the-art and the road ahead," *IET Communications*, Vol. 16, No. 13, 1458–1474, 2022.

[21] Zhu, J., Y. Xu, T. Ma, D. He, H. Li, Y. Guan, and W. Zhang, "RIS-assisted low complexity precoding for decentralized massive MU-MIMO system," *IEEE Transactions on Green Commu-*

nications and Networking, Vol. 10, 881–895, 2025.

[22] Mei, W., B. Zheng, C. You, and R. Zhang, "Intelligent reflecting surface-aided wireless networks: From single-reflection to multireflection design and optimization," *Proceedings of the IEEE*, Vol. 110, No. 9, 1380–1400, 2022.

[23] Costello, D. J., "Fundamentals of wireless communication (Tse, D. and Viswanath, P.)[Book review]," *IEEE Transactions on Information Theory*, Vol. 55, No. 2, 919–920, 2009.

[24] Wei, X., D. Shen, and L. Dai, "Channel estimation for RIS assisted wireless communications — Part I: Fundamentals, solutions, and future opportunities," *IEEE Communications Letters*, Vol. 25, No. 5, 1398–1402, 2021.

[25] Wu, Q. and R. Zhang, "Towards smart and reconfigurable environment: Intelligent reflecting surface aided wireless network," *IEEE Communications Magazine*, Vol. 58, No. 1, 106–112, 2020.

[26] Pala, S., O. Taghizadeh, M. Katwe, K. Singh, C.-P. Li, and A. Schmeink, "Secure RIS-assisted hybrid beamforming design with low-resolution phase shifters," *IEEE Transactions on Wireless Communications*, Vol. 23, No. 8, 10 198–10 212, 2024.

[27] Singh, K., P.-C. Wang, S. Biswas, S. K. Singh, S. Mumtaz, and C.-P. Li, "Joint active and passive beamforming design for RIS-aided IBFD IoT communications: QoS and power efficiency considerations," *IEEE Transactions on Consumer Electronics*, Vol. 69, No. 2, 170–182, 2023.

[28] Nwufo, C., O. Simpson, and Y. Sun, "Reconfigurable intelligent surfaces (RIS) and their role in next-generation wireless networks: An overview," *Transactions on Emerging Telecommunications Technologies*, Vol. 36, No. 6, e70164, 2025.

[29] Chen, Z., J. Tang, X. Y. Zhang, Q. Wu, G. Chen, and K.-K. Wong, "Robust hybrid beamforming design for multi-RIS assisted MIMO system with imperfect CSI," *IEEE Transactions on Wireless Communications*, Vol. 22, No. 6, 3913–3926, 2023.